Capacitation-associated alkalization in human sperm is differentially controlled at the subcellular level

Running title: Modulation of intracellular pH at the subcellular level during human sperm capacitation and its role in hyperactivated motility

Matamoros-Volante A. and Treviño C.L.*

Departamento de Genética del Desarrollo y Fisiología Molecular, Instituto de Biotecnología, Universidad Nacional Autónoma de México, Cuernavaca Morelos, México.

*Corresponding author: ctrevino@ibt.unam.mx.

Key words: sperm capacitation, intracellular pH, bicarbonate transport, Hv1 proton channel, hyperactivation.

Summary statement: Human sperm display differential pH_i regulation at the subcellular level upon capacitation, involving the participation of PKA kinase signaling pathway and several membrane transport proteins, culminating in hyperactivation.

ABSTRACT

Capacitation in mammalian sperm involves the accurate balance of intracellular pH (pH_i), but the underlying control mechanisms are not fully understood, particularly regarding the spatiotemporal regulation of the proteins involved in such pH_i modulation. Here we employed an image-based flow cytometry technique combined with pharmacological approaches to study pH_i dynamics at the subcellular level during sperm capacitation. We found that, upon capacitation induction, sperm cells undergo intracellular alkalization in the head and principal piece regions, but not in the midpiece. The observed localized pH_i increases require the initial uptake of

HCO_3^-, and it is mediated by several proteins acting in a manner consistent with their subcellular localization. Hv1 proton channel and cAMP-activated Protein Kinase (PKA) antagonists impair alkalization mainly in the principal piece. Na^+/HCO_3^- cotransporter (NBC) and cystic fibrosis transmembrane regulator (CFTR) antagonists impair alkalization only mildly, predominantly in the head. Motility measurements indicate that inhibition of alkalization in the principal piece prevents the development of hyperactivated motility. Altogether, our findings shed light into the complex control mechanisms of pH_i and underscore their importance during human sperm capacitation.

INTRODUCTION

The concentration of H^+ is a ubiquitous regulatory element for most biochemical reactions and it has relevance in many physiological processes, including sperm function (Nishigaki et al., 2014). It has been widely recognized that mammalian sperm must undergo a series of maturation steps in order to develop full fertilizing capabilities; such processes are collectively known as capacitation, and in vivo they only take place once sperm are inside the female reproductive tract (Austin and Sakkas, 1951; Chang, 1951). Intracellular pH (pH_i) plays a pivotal role in capacitation, controlling various key proteins involved in it. For example, an increase in pH_i promotes the activation of KSper currents (Navarro et al., 2007), which are mediated by the SLO3 K^+ channel (Zeng et al., 2011; Zeng et al., 2013). SLO3 expression is restricted to sperm cells, and *Slo3* knockout male mice are infertile. Although the mechanisms behind this infertility are not completely understood,

failure to fertilize is related to a reduction in progressive motility and an impairment of the acrosomal exocytosis process in sperm (Santi et al., 2010).

Additionally, pH_i mediates the development of hyperactivated motility, a special kind of sperm movement characterized by asymmetrical flagellar beating, and which is necessary for successful fertilization (Mishra et al., 2018; Suarez, 2008). Such hyperactivation is mediated by CATSPER, a sperm-specific Ca^{2+} channel that is activated by alkaline pH_i through interaction with EFCAB9, a pH-tuned Ca^{2+} sensor that controls CATSPER gating (Hwang et al., 2019). Notably, loss-of-function mutations on any of the CATSPER channel subunits cause infertility in male mice (Qi et al., 2007; Ren et al., 2001) and humans (Avenarius et al., 2009), mainly due to the inability of sperm to hyperactivate. It is widely recognized that pH_i regulation in mice sperm involves the participation of another sperm-specific protein, the Na^+/H^+ exchanger (sNHE), which drives H^+ extrusion employing the cell's $[Na^+]$ gradient. Similar to CATSPER and SLO3, the lack of sNHE results in male infertility (Wang et al., 2003). While humans express an orthologous sNHE gene, its involvement in human sperm physiology remains elusive. In this regard, the proton channel (Hv1) has been proposed as the main pH_i regulator during human sperm capacitation and hyperactivation (Lishko et al., 2010), and its activity has been linked to the activation of CATSPER, leading to Ca^{2+} influx and the concomitant changes in motility patterns (Lishko and Kirichok, 2010; Miller et al., 2015) (Lishko and Kirichok, 2010; Miller et al., 2018). Interestingly, the subcellular localization of all aforementioned proteins is restricted to the flagellum, particularly the principal piece region, which is consistent with their role in motility. On the other hand, our group and others have described the expression and participation of an additional set of proteins during mammalian

sperm capacitation, which are related to HCO_3^- transport and thus could potentially participate in pH_i balance as well. These proteins include members of the SLC26 (Chávez et al., 2012; El Khouri et al., 2018) and SLC4 (Demarco et al., 2003; Parkkila et al., 1993; Puga Molina et al., 2018; Zeng et al., 1996) HCO_3^- transporter families. One member of the SLC4 family, namely the electrogenic Na^+/HCO_3^- cotransporter (NBC), appears to mediate HCO_3^- influx, which is required for downstream activation of signaling networks essential for capacitation, such as the cAMP-activated Protein Kinase (PKA) pathway (Demarco et al., 2003; Puga Molina et al., 2018). This particular pathway also seems to mediate plasma membrane hyperpolarization, a hallmark of capacitation, via stimulation of the Cystic Fibrosis Transmembrane Regulator (CFTR) Cl^-/HCO_3^- channel (Chávez et al., 2012; Hernández-González et al., 2007; Puga Molina et al., 2017). Interestingly, pharmacological blocking of CFTR impairs capacitation in mice (Li et al., 2010; Xu et al., 2007) and human (Puga Molina et al., 2017) sperm. Also, its genetic ablation produces subfertility in mice (Xu et al., 2007). Notably, the subcellular localization of these HCO_3^- transporters differs from that of the H^+ extruders (i.e. Hv1 and sNHE), with some of the former being mainly localized in the head, and to some extent in the midpiece, but not in the principal piece (Liu et al., 2012; Nishigaki et al., 2014). This suggests that pH_i might be differentially regulated throughout the cell, presumably through the participation of different proteins.

A few studies have provided evidence of the net pH_i increase that occurs during capacitation, by measuring initial and end point pH_i (Cross and Razy-Faulkner, 1997; Lopez-Gonzalez et al., 2014). But despite the importance of pH_i in sperm physiology, there have been no examinations of pH_i kinetics throughout the entire capacitation

process, nor have they been tracked in distinct sperm cell regions. Conducting such studies in sperm cells poses unique experimental challenges given their complex morphology, motility and asymmetrical anatomy, which results in highly compartmentalized physiological cell signals (Buffone et al., 2012).

We recently developed a completely novel strategy to analyze intracellular events in a statistically relevant number of cells, using image-based flow cytometry along with a segmentation process that provides spatial resolution within individual sperm cells (Matamoros-Volante et al., 2018). In the present work, we employed this technique to investigate pH_i kinetics at the subcellular level during human sperm capacitation. We found that, upon the cells' contact with capacitation medium, pH_i remained constant in the midpiece, while it increased in the head and in the principal piece, displaying different kinetics. Using pharmacology, we found that multiple proteins mediate the observed pH_i changes, with their involvement being distinct in the head and in the principal piece. Lastly, motility measurements indicated that these proteins are required for hyperactivation, but not to maintain total motility. Altogether, our results suggest that pH_i modulation in human sperm involves the participation of an entire set of proteins, with the pH_i changes being orchestrated in a localized, and possibly time-dependent fashion.

RESULTS

During capacitation, pH_i increases in the head and in the principal piece, but not in the midpiece. While a pH_i increase has been widely recognized as a hallmark of sperm capacitation (Nishigaki et al., 2014), the dynamics and subcellular localization of this alkalization, to our knowledge, had not been previously explored. We employed the pH-sensitive fluorescent probe BCECF to track subcellular pH_i

changes in human sperm cells using an image-based flow cytometer (Fig. S3A-B). To demonstrate that our previously reported segmentation process (Matamoros-Volante et al., 2018) was suitable for measuring pH_i changes in distinct sperm cell regions (Fig. S3C-D), we exposed BCECF-loaded sperm cells to an alkalizing agent (20 mM trimethylammonium, TMA) known to produce a sustained pH_i increase of around 0.4 units (Alasmari et al., 2013). As described in Materials and Methods, cell regions were arbitrarily considered to have a high pH_i if their fluorescence value was higher than those of the third quartile in the NC condition. Then, in order to determine whether any given treatment had an alkalizing effect on pH_i, the change in the percentage of subcellular regions with high pH_i (Δ%) was calculated with respect to that of the corresponding NC condition, after having eliminated outliers (i.e. those in the top 5%). When cells were exposed to 20 mM TMA, we observed a reproducible increase in the percentage of cells exhibiting high pH_i (Δ%) in each of the three distinct subcellular regions analyzed, i.e. head, midpiece and principal piece (Fig. S3E). The pooled fluorescence values for all subcellular regions analyzed for all sperm donors are also shown as boxplots (Fig. S3F). With both approaches used for data analysis, the observed localized pH_i increases caused by TMA exposure were statistically significant for all three cell regions, confirming the reliability of our technique

We then studied the pH_i dynamics in each subcellular region during capacitation, triggered by exposure to capacitation medium (Fig. 1). Representative images of cells at different capacitation time points are shown in Fig. 1A. As seen in Fig. 1B, there was a significant increase in the percentage of cells with high head pH_i (hd-pH_i) after the initial exposure to capacitation medium (t=0 min), (Δ%=17, p<0.0001).

143 Δ% reached a maximum after 15 minutes (Δ%=21, p<0.0001), and although it
144 gradually dropped and leveled off at Δ%~16, the increase in the percentage of cells
145 with high hd-pH_i was statistically significant up to 240 minutes of capacitation
146 (p<0.0001). Similar dynamics were observed when the pH_i was measured in the
147 principal piece (pp-pH_i), though the changes in Δ% were not as pronounced (Fig.
148 1B). The increase in the percentage of cells with high pp-pH_i became statistically
149 significant only after 15 minutes of capacitation (Δ%=10, p=0.0023), reaching a
150 maximum at 30 minutes (Δ%=15, p=0.003). Δ% value then dropped to ~9 after 45
151 minutes and remained essentially constant up to 240 minutes of capacitation, though
152 the increase in Δ% was no longer statistically significant throughout this time period.
153 In contrast, the change in the percentage of cells with high midpiece pH_i (mp-pH_i)
154 consisted overall of a slight and gradual decrease throughout the entire capacitation
155 period analyzed, though the observed differences were never statistically significant
156 (Fig. 1B). These results display similar statistics when the pooled fluorescence
157 values for all the subcellular regions measured from all donors are analyzed as
158 boxplots (Fig. 1C). The fact that, unlike the other two subcellular regions, the mp-pH_i
159 remained unchanged was rather surprising to us, and even though we were able to
160 detect a statistically significant pH_i increase in the midpiece using TMA (Fig. S3E),
161 we wanted to verify that this was not simply due to a limitation in our experimental
162 methodology, which could potentially be preventing the reliable detection of
163 fluorescence changes in the midpiece. To this end, we incubated sperm cells with
164 250 nM MitoTracker Green FM, a mitochondrial-specific fluorescent dye that has
165 been employed as a marker for membrane mitochondrial potential (Sousa et al.,
166 2011). We then triggered a change in fluorescence by challenging these cells with 1

μM CCCP (carbonyl cyanide m-chlorophenyl hydrazine), a mitochondrial electron transport system disrupter. A clear reduction of MitoTracker fluorescence was detected in the midpiece (data not shown), thus indicating that our mp-pH_i measurements are reliable. Given that no significant changes in mp-pH_i were detected during capacitation, we decided to analyze only the head and principal piece regions in all further pH_i dynamics studies.

Before proceeding any further, however, we wanted to verify that our experimental conditions were not causing cell damage due to BCECF phototoxicity, even though this was not expected to occur since cells were illuminated for a very short time (milliseconds) during data acquisition. However, BCECF was present in the cell samples up to 6 hours of capacitation, with aliquots being taken for measurements at different time points. To explore whether this exposure was deleterious to the cells, we used PI as a marker for viability. We did not find change in the percentage of viable cells after either 1 or 6 hours of incubation with BCECF, compared to the NC unstained cells (Fig. S4A). Additionally, we wanted to exclude the possibility that any measured pH_i increases were simply caused by the time that cells spent in incubation. To this end, we incubated cell samples during 1 and 6 hours in a NC medium. As seen in Fig. S4B-C, no significant changes in pH_i were observed at either of these two time points in any of the three subcellular regions. Altogether, these data indicate that the observed pH_i increases are a result of incubation in the presence of capacitation medium.

Absence of HCO_3^- or blockage of HCO_3^- influx prevent pH_i increases during capacitation in both the head and the principal piece. When sperm are ejaculated they are exposed to a higher extracellular concentration of HCO_3^- (Owen

and Katz, 2005), which is mimicked *in vitro* through exposure to capacitation medium (25 mM HCO_3^-, similar to the concentration found in the seminal fluid and the female reproductive tract). To explore the role of HCO_3^- in the observed pH_i changes, we incubated sperm in either an incomplete capacitation medium lacking HCO_3^- (no HCO_3^-), or in complete capacitation medium containing 100 µM DIDS, a general inhibitor of anionic transporters, to block HCO_3^- entry through channels and transporters at three capacitation times (0, 60 and 240 min). Under both conditions, the pH_i increase was completely abolished in the head and in the principal piece (Fig. 2A-C, Fig. S2A). Statistical analysis of both the average Δ%A values and the pooled fluorescence values for all subcellular regions analyzed from all donors yielded comparable statistically significant differences. These results suggest that HCO_3^- uptake via anionic transporters is necessary to induce the rise in pH_i in both sperm regions.

NBC and CFTR have a minor role in cytoplasmic alkalization during capacitation in the head, but not in the principal piece. Previous results from our group have demonstrated that upon HCO_3^- exposure, sperm cells become hyperpolarized due to HCO_3^- uptake mediated by an electrogenic NBC (Demarco et al., 2003; Puga Molina et al., 2018). We thus explored whether pharmacological inhibition of NBC proteins could also prevent pH_i increases during capacitation. Interestingly, the mere pre-incubation (10 min) of sperm under NC conditions with a specific antagonist of NBC proteins (S0859, 5 µM) (Ch'en et al., 2008), provoked acidification in the head (Δ% = -11, p = 0.0096) compared to NC conditions (Fig. S2B). During capacitation, NBC blockage did not prevent the pH_i increases in the head nor in the principal piece (Fig. 3A-B).

Previously, we reported that pharmacological blocking of CFTR produces cytoplasmic acidification after 5 hours of capacitation (Puga Molina et al., 2017). Since this channel can also transport HCO_3^- into the cell, we used Inh-172, a specific CFTR antagonist, to explore the role of CFTR in the observed alkalization of subcellular regions. During capacitation, there is a decrease in the percentage of cells with high hd-pH_i, though it is statistically significant only at 240 min (Fig. 3A-B). Inhibition of CFTR did not affect the pH_i increase in the principal piece (Fig. 3A-B, Fig.S2B). Although pre-incubation with Inh-172 also caused a reduction in Δ% under NC conditions both in the head and principal piece, it was not statistically significant in these cases (Fig. S2B)

PKA signaling pathway participates in the regulation of capacitation-associated alkalization in the principal piece, but not in the head. The above observations suggest that HCO_3^- influx is indispensable for the initial and sustained pH_i increases, which are stable during at least during 4 hours of capacitation. HCO_3^- is a key component of capacitation medium, and is known to activate a PKA pathway leading to important changes during capacitation (Buffone et al., 2014). It is well accepted that a HCO_3^- influx stimulates cAMP production via a HCO_3^--sensitive adenylyl cyclase (ADCY10) with the subsequent PKA activation (Okamura et al., 1985). Additionally, Puga-Molina, et al. (2017), showed that pharmacological blocking of PKA with H89 induces cytoplasmic acidification in human sperm, measured after 5 h of capacitation. We wondered whether the HCO_3^- requirement for alkalization that we observed is linked to PKA pathway activation. We tested this possibility by incubating sperm with either H89 (30 µM), a PKA inhibitor, or KH7 (50 µM) an ADCY10 antagonist. While neither inhibitor affected Δ%A in the head during

capacitation (Fig. 4A-B), both diminished it in the principal piece, though the decrease was statistically significant only at 240 min (p=0.032 and 0.0285 respectively) (Fig. 4A). However, when fluorescence data are compared through boxplots (Fig. 4B), the reduction in the BCECF fluorescence in the principal piece was statistically significant at all capacitation time points (p<0.0306) for H89, and only at 240 min for KH7 (p=0.0182). Additionally, preincubation under NC conditions with H89 reduced Δ% of cells with high pp-pH_i (Fig. S2C).

Inhibition of Hv1 prevented alkalization in the principal piece but not in the head. Previous reports have demonstrated that, upon capacitation, Hv1 activity increases in human but not in mice sperm (Lishko et al., 2010). We thus tested whether Hv1 were involved in the observed increases in hd-pH_i and pp-pH_i by incubating cells with 200 µM Cl-GBI, a specific Hv1 antagonist (Hong et al., 2014). Cl-GBI had no significant effect on Δ%A in the head (Fig. 5A-B, Fig. S2D). Cl-GBI, induced a strong reduction in Δ%A in the principal piece at all incubation times (p<0.0387) (Fig. 5A-B) as well as an acidification when preincubated under NC conditions (p=0.0482) (Fig. S2D).

To further confirm Hv1 participation in the pH_i increase, we used Zn^{2+}, a well-known inhibitor of Hv1. The presence of 200 µM of ZnCl (Zn^{2+}) reduced significantly Δ%A in the head at 240 min (p=0.0286) of capacitation (Fig. 5A) which was also observed when pooled fluorescence values were analyzed (p=0.0245) (Fig. 5B). The pH_i increase was strongly inhibited by Zn^{2+} in the principal piece at all capacitation times (p<0.0339), the reduction was significant regardless of the analysis (Fig. 5A-B). These data confirm the participation of Hv1 in human sperm pH_i regulation, but also

corroborate that at least in the head other proteins must be participating in the control of pH_i in that cell region.

Proteins that regulate pH_i are required for hyperactivation. The downstream role of HCO_3^- uptake in the control of sperm hyperactivation has been widely recognized (Okamura et al., 1985), primarily via a PKA signaling pathway and CATSPER activation (Orta et al., 2018; Qi et al., 2007; Wennemuth et al., 2003). In this work we showed that Hv1, HCO_3^- influx, and to a lesser extent CFTR, are required for the pH_i increases during capacitation. Employing a CASA system, we explored whether inhibition of these proteins and the lack of HCO_3^- affected sperm hyperactivation. Interestingly, none of these conditions produced a change in total motility compared to control conditions during the explored time window (Fig. 6A). In contrast, all these treatments caused, to varying degrees, reduction in the percentage of cells that displayed hyperactivated motility, compared to control conditions. For instance, both Hv1 inhibition and the absence of HCO_3^- in the medium completely prevented hyperactivation (p<0.0310) (Fig. 6B). CFTR blocking significantly reduced hyperactivation at 0 min, 60 and 240 min (p=0.0193) (Fig. 6B) and inhibition of NBC reduced the number of hyperactived cells (p< 0.0001) upon capacitation induction (0 min), but not after 60 and 240 min.

Lastly, we plotted the percentage of cells exhibiting hyperactivated motility as a function of the percentage of cells with high pp-pH_i. We found that hyperactivation increases exponentially as a function of alkalization in the principal piece (R^2=0.80, $y = 7.686e^{(0.007X)}$, $\tau = 12.85$). (Fig. 6C).

DISCUSSION

Through comparisons of initial and final pH_i, *in vitro* studies have shown that human sperm cells exhibit alkalization after 24 (Cross and Razy-Faulkner, 1997) and 13 (Lopez-Gonzalez et al., 2014) hours of capacitation. More recently, while we were preparing the present manuscript for publication, Brukman and colleagues reported that pH_i in a human sperm subpopulation increased slightly after 10 min of capacitation, had a further increase after 1 hour, and then remained constant after 2, 4 and 6 hours (Brukman et al., 2019). These observations were made employing conventional flow cytometry on BCECF-stained cells. For the present study, we applied our recently developed sperm segmentation process using image-based flow cytometry (Matamoros-Volante et al., 2018) to follow human sperm pH_i changes in three distinct subcellular regions (head, midpiece and principal piece) at various time points of capacitation (up to 4 hours). We started out by demonstrating that this method can be reliably used to detect pH_i changes in all three regions.

As expected, histograms constructed on BCECF fluorescence values measured for each sperm population sample vary in distribution and amplitude across donors and experimental replicates, even under equal treatment conditions. The fluorescence data sets from all donors/replicates were first pooled and displayed as boxplots for every given condition, enabling comparisons and statistical analyses. For each of them, in addition, the percentage of subcellular regions having fluorescence values above those of the third quartile of the NC control was calculated. These values were then plotted as a percentage difference with respect to control conditions in order to display and compare the pH_i kinetics during capacitation.

We observed that under conditions that do not support capacitation, pH_i in all three subcellular regions remained constant over the 4-h time window. But when sperm were incubated under conditions that promote capacitation, a pH_i increase occurred in the head and principal piece, remaining stable during the entire time window studied. Given that no change in midpiece pH_i was observed, further analyses of the proteins involved in regulating pH_i were conducted solely in the head and principal piece.

Previous evidence obtained by our group suggests that an electrogenic NBC is responsible for HCO_3^- influx during capacitation (Demarco et al., 2003; Puga Molina et al., 2018). In the present work, we observed that pharmacological inhibition of NBC caused a decrease in basal pH_i under NC conditions both in the head and principal piece. However, upon addition of capacitation medium, Δ%A was very similar to Δ% in both subcellular regions. These results indicate that NBC participates in pH_i homeostasis prior to capacitation, rather than having a role in the pH_i increase observed during capacitation, and they also suggest that other proteins are responsible for such increase.

Recently, our group also proposed that HCO_3^- influx might either take place directly through CFTR, or through other transporters coupled to CFTR (Puga Molina et al., 2017; Puga Molina et al., 2018). In the earlier manuscript, based on conventional flow cytometry measurements, we reported that CFTR inhibition causes a decrease in pH_i after 5 hours of capacitation. While our present results indicate that CFTR inhibition caused only a slight pH_i decrease in the head and principal piece, it was statistically significant in the head at 4 hours of capacitation, in agreement with our previous measurements performed after 5 hours of capacitation. We had previously

proposed that the increase in pH_i during capacitation could be due to the concerted action of NBC and CFTR (Puga Molina et al., 2017; Puga Molina et al., 2018). Our present results indicate that, at least for the initial pH_i increase, NBC and CFTR are not required.

On the other hand, both the absence of HCO_3^- and the general blocking of HCO_3^- transporters completely prevented the pH_i increase in both subcellular regions. These results suggest the participation of additional proteins with HCO_3^- transport activity. In this regard, HCO_3^- transporters from the NBC family, such as the electroneutral Na^+-driven Cl^-/HCO_3^- exchangers, NDCBE (SLC4A8) and NBCn2 (SLC4A10) have been detected in human testis, albeit only at the transcriptional level (Damkier et al., 2007; Pushkin et al., 2000). Additionally, other proteins related to HCO_3^- transport have been found in mammalian sperm, such as the SLC26 family members A3 and A6 (Chávez et al., 2012; El Khouri et al., 2018), as well as A8 (Touré et al., 2007), and carbonic anhydrase activity has also been detected in human sperm (José et al., 2015; Wandernoth et al., 2010). Further research is needed to investigate whether these other transporters/enzymes are involved in pH_i regulation.

The evidence provided here suggests that different proteins are involved in pH_i regulation in different sperm subcellular regions. We propose that HCO_3^- transporters in the head (yet to be identified) are responsible for the initial and sustained HCO_3^- uptake. It is then possible that diffusion of HCO_3^- (or a second messenger) occurs from the head to the flagellum, which would explain the delay in pH_i increase observed in the principal piece between, compared to the head.

355 The initial HCO_3^- influx, known to activate a PKA pathway, could presumably also
356 participate in the initial pH_i increase. According to previous studies conducted by our
357 group, PKA blockage with H89 causes strong cytoplasmic acidification in
358 capacitated human sperm (Puga Molina et al., 2017). Using this same inhibitor and
359 KH7, our present results corroborate participation of the PKA pathway on pH_i
360 regulation, with a major contribution in the principal piece and, to a lesser extent, in
361 the head. PKA localization in human sperm is not restricted to a specific site
362 (Neuhaus et al., 2006), but the main subcellular localization of PKA substrates are
363 in the principal piece (Battistone et al., 2013).
364 Previous work has established that in human sperm, Hv1 mediates outward H^+
365 currents, which are enhanced once sperm are capacitated (Lishko et al., 2010). We
366 found that pharmacological inhibition of Hv1 with both Cl-GBI and Zn^{2+} does prevent
367 alkalization, in the principal piece, but leaves alkalization in the head unaltered.
368 These results are consistent with the reported localization of this channel exclusively
369 in the principal piece (Lishko et al., 2010; Miller et al., 2018). The fact that Hv1
370 blockage does not prevent the pH_i increase in the head, suggests that Hv1 is not the
371 sole pH_i regulator in human sperm, and other mechanisms are likely at work in order
372 to generate such alkalization in the head. Unexpectedly, the presence of Zn^{2+}
373 caused a reduction of pH_i in the head after 4 hours of capacitation. This effect is
374 presumably due to a Zn^{2+} target other than Hv1, since it was not observed with the
375 specific Hv1 inhibitor Cl-GBI. Although Zn^{2+} is important for sperm physiology, little
376 is known about the Zn^{2+} transporters that operate in human sperm. Nonetheless, the
377 presence of at least some members from the Zip and ZnT families has been
378 described (Foresta et al., 2014). Transport of Zn^{2+} in and out the cell is generally

coupled to the transport of another ion. The Zip protein family consists of symporters that couple Zn^{2+} entry together with HCO_3^-. Given that the medium used to induce capacitation *in vitro* contains a high concentration of HCO_3^-, it is conceivable that the addition of Zn^{2+} enables such cotransport activity to take place. If this is the case, once Zn^{2+} accumulates in the cell, it could potentially be extruded via ZnT transporters. These function as antiporters with H^+, thereby explaining the observed acidification in the head at 4 hours of capacitation. Interestingly, we observed that inhibition of Hv1 causes a decrease of pH_i in the principal piece, even under conditions that do not promote capacitation, suggesting that this channel is also active and participates in pH_i regulation prior to capacitation.

Inhibition of Hv1 abolishes alkalization in the principal piece throughout the entire capacitation time window explored, rather than just initially. The existence of a mechanism maintaining Hv1 activity is therefore expected. It has been reported that Hv1 function is upregulated by phosphorylation of some of its serine and threonine residues, presumably by PKC (Hondares et al., 2014; Morgan et al., 2007; Musset et al., 2010). Thus, PKC could potentially be the key player necessary to sustain Hv1 activity during capacitation. PKC is present in human sperm flagella (Kalina et al., 1995), and its activity has been related to sperm motility (Rotem et al., 1990). Additionally, different lines of evidence along with recent work by Brukman and colleagues (Brukman et al., 2019) suggest a possible link between PKA and Hv1 activation during capacitation. Such activation likely involves the participation of other kinases, since direct Hv1 phosphorylation by PKA has not been demonstrated. During capacitation, there is an increase in tyrosine phosphorylation (PY) of different proteins, which occurs downstream of PKA activation, mainly in the sperm tail

(Battistone et al., 2013). This process involves the action of at least two different tyrosine kinases (TKs), PYK2 and FER(T) (Alvau et al., 2016; Battistone et al., 2014; Matamoros-Volante et al., 2018). Brukman et al., 2019 showed that the pharmacological inhibition of these TKs blocks the capacitation-associated alkalization in human sperm cells, and they proposed a possible a connection between TKs and PKC, which in turn upregulates Hv1 (Brukman et al., 2019). Evidence from other cell types suggests that H^+ conductance driven by Hv1 is also affected by PY, for example in granulocytes (Bianchini et al., 1994) and in neutrophils (Nanda and Grinstein, 1995), although the identity of the implicated TKs remains unknown. Altogether, these findings suggest that Hv1 might be regulated by a signaling network involving PKA, PKC and TKs. Additional experiments are needed to support this proposal.

One of the most important downstream effects of HCO_3^- uptake is the induction of a change in sperm motility patterns (Hereng et al., 2014; Wennemuth, 2003). In fact, sperm from infertile patients present low HCO_3^- levels in seminal plasma, which correlates with poor sperm motility (Okamura et al., 1986). HCO_3^- effects on motility are controlled in a Ca^{2+}-dependent manner (Ho et al., 2002; Marquez and Suarez, 2007). The sperm-specific alkalization-dependent calcium channel, CATSPER, is the main molecular entity responsible for intracellular [Ca^{2+}] changes upon capacitation (Kirichok *et al.*, 2006). Genetic ablation of *CatSper* produces infertility because sperm fail to hyperactivate (Qi et al., 2007). In some models, the intracellular alkalization mediated by Hv1 has been proposed to act as a signal that opens CATSPER, in turn triggering and maintaining hyperactivated motility (Lishko and Kirichok, 2010). Besides, proteins of the glycolytic machinery related to ATP

427 production are required to sustain hyperactivation and the dynein-ATPase
428 necessary to axonemal functionality is also pH_i dependent (Mannowetz et al., 2012;
429 Ui, 1966). Altogether, the available evidence suggests a tight relationship between
430 pH_i and sperm hyperactivation. In the present work, we demonstrate for the first time
431 that pharmacological inhibition of Hv1 reduces hyperactivation, while leaving total
432 motility unchanged. In fact, with the exception of NBC inhibition, the effect on
433 hyperactivation brought about by our experimental treatments always mirrors their
434 effect on pH_i in the principal piece. In other words, conditions that completely prevent
435 alkalization in the principal piece (i.e. either Cl-GBI or medium lacking HCO_3^-) also
436 reduce hyperactivated motility. Conversely, CFTR inhibition, which elicits a minor
437 decrease on pH_i, reduces hyperactivation only slightly. Such a correlation is not
438 apparent upon NBC inhibition, as hyperactivation does not occur, even though the
439 pH_i increase in the principal piece is similar in magnitude as the one observed under
440 control conditions. In this case, however, mere preincubation with the inhibitor
441 causes an initial reduction in pH_i prior to capacitation, and it is thus conceivable that
442 despite alkalization occurring during capacitation, pH_i does not reach the necessary
443 threshold to promote hyperactivation. Thus, while we found the relationship between
444 hyperactivation (%) and pH_i increase in the principal piece to be exponential,
445 alkalization might need to be high enough to reach a certain threshold in order for
446 hyperactivation to occur.
447 In summary, we have shown that cytoplasmic $[H^+]$ in human sperm is differentially
448 controlled in the head and principal regions; this process involves the participation
449 of various proteins, acting under distinct spatiotemporal control mechanisms.
450 Additionally, our results further support the notion that intracellular alkalization plays

a key role in the control of sperm motility. The findings reported here highlight the complexity and relevance of pH_i dynamics during human sperm capacitation.

MATERIALS AND METHODS

Materials

Potassium dihydrogen phosphate (KH_2PO_4) and anhydrous glucose were obtained from J.T. Baker (USA). Bovine Serum Albumin (BSA) was purchased from US Biological (USA). 2',7'-Bis-(2-carboxyethyl)-5-(and-6)-carboxyfluorescein, acetoxymethyl ester (BCECF-AM), MitoTracker Green FM, and propidium iodide (PI) were obtained from Invitrogen (USA). CFTR-Inh-172 was purchased from Calbiochem Inc. (USA). 2-Chloro-N-[[2′-[(cyanoamino) sulfonyl] [1,1′-biphenyl]-4-yl] methyl]-N-[(4-methylphenyl) methyl]-benzamide, known as S0859, was obtained from Cayman Chemical (USA). 2-guanidinebenzimidazole (2-GBI), 5-chloro-2-guanidinebenzimidazole (Cl-GBI), 4,4′-Diisothiocyanatostilbene-2,2′-disulfonic acid disodium salt hydrate (DIDS), N-[2-(p-Bromocinnamylamino)ethyl]-5-isoquinolinesulfonamide dihydrochloride (H89), zinc chloride (Zn^{2+}) and (E)-2-(1H-benzo[d]imidazol-2-ylthio)-N′-(5-bromo-2-hydroxybenzylidene) propanehydrazide (KH7) were obtained from Sigma-Aldrich (USA), along with all other chemicals.

Ethical Approval

Protocols for human sperm use were approved by the Bioethics Committee of the Instituto de Biotecnología (UNAM, México). Informed consent forms were signed by all donors.

Culture media

The non-capacitating (NC) medium used in this study was HEPES-buffered Human Tubal Fluid (HTF) Solution containing (in mM): NaCl 90.69, KCl 4.67, $CaCl_2$ 1.6, $MgSO_4$ 1.2, KH_2PO_4 0.314, Glucose 2.78, Na-Pyruvate 3.38, Na- lactate 60, Hepes 23.8. Capacitation-inducing conditions consisted of HTF medium supplemented with 25 mM $NaHCO_3$ and 5% BSA (w/v). All media were adjusted to pH 7.4 with HCl, and the osmolarity was maintained at around 290 mOs kg^{-1}.

Sperm

Sperm samples were obtained from healthy donors, collected by masturbation after 3-5 days of sexual abstinence. Only those samples with normal seminal parameters (according to the 2010 WHO criteria) were used in the study. Semen samples were liquefied for 30 min at 37°C under an atmosphere of 5% CO_2 in air. Motile sperm were obtained by the swim-up technique, employing NC medium for 1 h at 37°C under an atmosphere of 5% CO_2 in air. A Makler® Counting Chamber (Sefi Medical Instruments, Israel) was used to adjust the sperm concentration at $10x10^6$ cells/mL. Sperm samples in NC medium were loaded with 250 nm BCECF-AM (see below) and then incubated during 15 min at 37°C, protected from light. Excess dye was removed by centrifugation at 300 g for 5 min, and the cell pellet was resuspended in NC medium to obtain a sperm concentration of 2-8 x 10^6 cells/mL. For pharmacology evaluations, these BCECF-AM-loaded cells were pre-incubated for 10 min with the various blockers tested (5 µM of either Inh-172 or S0859, 100 µM DIDS, 50 µM of KH7, 30 µM H89, 200 µM of Cl-GBI and 200 µM Zn^{2+}) or with the vehicle (DMSO or culture media) alone (control). After pre-incubation, an aliquot of cells was combined with an equal volume of 2X capacitation medium (supplemented with the same

concentrations of the different blockers), and sperm cells were incubated at 37°C under a 5% CO_2 atmosphere. At different time periods, up to a maximum capacitation time of four hours, an aliquot of cells was taken for analysis.

Intracellular pH estimation by image-based flow cytometry

Intracellular pH (pH_i) was monitored through fluorescence measurements using the pH-sensitive cell-permeable probe BCECF-AM. Once this dye enters the cell, cytosolic estereases cleave the acetoxymethyl ester (AM) group and free BCECF accumulates in the cell's cytosol. The intensity of this dye's fluorescence emission (λ=535 nm) increases with increasing pH, enabling the tracking of pH_i conditions. BCECF-loaded cells, in either NC or capacitation medium were concentrated from 2 x 10^6 to 8 x 10^6 cells/mL (in a final volume of 50 µL) by centrifugation at 300 g for 5 min. At least 30 seconds before measurements, 250 nM PI (final concentration) was added to the cell suspension to evaluate sperm viability. BCECF and PI fluorescence were measured using the image-based flow cytometer ImageStream Mark II (Amnis, USA). The acquisition settings of INSPIRE® software (Amnis, USA) were as follows: objective: 60X magnification, excitation laser: 488nm, laser intensity range: 20-100 mW (in order to avoid over excitation and pixel saturation), BCECF emission: 535nm, collected in channel 2 (range 480-560 nm), PI emission: 620 nm, collected in channel 4 (range 595-660 nm), brightfield images: channel 1. During acquisition, different parameters were set for preliminary discrimination of saturated, cell aggregates, non-sperm (*e.g*. round cells), and non-focused cells according to previous work (Matamoros-Volante et al., 2018). After pre-processing, 12,500 cells were recorded for each condition.

519 To estimate the kinetics of pH_i changes during capacitation, we employed the
520 aforementioned conditions to assess BCECF fluorescence under NC conditions (*i.e.*
521 after swim-up and dye loading). For measurements under capacitation conditions,
522 recordings were done immediately after the addition of 2X capacitation medium
523 (considered capacitation time = 0 min). Thereafter, we tracked pH_i under
524 capacitation conditions at 15-min intervals, up to 180 min of incubation, unless
525 otherwise specified. A final measurement was made at 240 min of capacitation.

526 **Computer assisted sperm analysis (CASA)**

527 The effect of the various blockers in sperm motility was evaluated using a CASA
528 system. A 7-µL aliquot of each sperm sample was placed in a pre-warmed
529 microscopy slide, covered with a coverslip (18 x 18 mm), and sperm motility was
530 monitored using a negative phase contrast 10X objective (Nikon, Japan). Data was
531 acquired using Sperm Class Analyzer software (SCA, Microptics, Barcelona, Spain).
532 500 cells were measured for each experimental condition, by collecting 25 images
533 with a frequency of 50 Hz. Sperm hyperactivation was assessed according to the
534 criteria established by Mortimer, 2000, as follows: curvilinear velocity (VCL): > 150
535 µm/s; linearity (LIN): < 50%; half lateral head displacement ($ALH_{1/2}$): > 3.5 µm.

536 **Image based-flow cytometry data analysis**

537 Image-based flow cytometry-derived images were analyzed with IDEAS® software
538 version 6.2 (Amnis, USA) using a previously reported analysis strategy designed to:
539 a) discriminate non-sperm events (doublets, debris, etc.), unfocused images, and
540 dead cells (positive to PI); and b) perform segmentation of sperm images in order to

541 selectively analyze three distinct sperm cell regions, namely the head, the midpiece,
542 and the principal piece (Matamoros-Volante et al., 2018). After completing the
543 formerly described selection and segmentation processes, anywhere between 1,000
544 and 2,000 cell regions per treatment remained for analysis from each of the semen
545 samples (n=3 to 9). For each treatment, fluorescence histogram data (*e.g*. Fig.S1A)
546 from the various semen samples were pooled into boxplots (*e.g*. Fig. S1B) for each
547 of the three analyzed cell regions. In order to identify pH_i increases across sperm
548 populations subjected to various treatments and/or capacitation time points, only cell
549 regions exhibiting a fluorescence value higher than those of the third quartile in the
550 NC condition (i.e. falling to the right of the dashed line in Fig. S1A-B) were arbitrarily
551 considered as having a high pH_i. The percentage of such high pH_i cell regions (Fig.
552 S1B) was then calculated for the NC condition (%NC) and for each treatment/time
553 point (%T), after eliminating outliers (i.e. those with fluorescence values in the top
554 5%). To assess the effect of each capacitation time point (%T) or treatment ($\%T_A$),
555 the difference between those percentages (Δ%) was calculated as follows: Δ%=%T-
556 %NC (*e.g*. Fig. S1C). In many cases, the %NC value under altered conditions
557 ($\%NC_A$) (i.e. absence of HCO_3^- or presence of a blocker) was significantly lower than
558 that of %NC (*e.g*. Fig. S1B-C), resulting in negative Δ% values (*e.g.* Fig. S1C). To
559 enable side-by-side comparisons of pH_i kinetics, we adjusted Δ% values for altered
560 conditions to start at zero (*i.e.* equal to the NC condition) through an alternative
561 calculation: $\Delta\%A = \%T_A - \%NC_A$ (*e.g.* Fig. S1D). With this normalization, the effect of
562 each treatment is measured with respect to its corresponding initial NC condition
563 (NC or NC_A). However, in order to appreciate the effect of pre-incubation with
564 blockers on the initial $\%NC_A$ value, we also show all pHi kinetics plots using %NC

565 for all Δ% calculations (Fig. S2A-D, see corresponding normalized results in Figures
566 2A, 3A, 4A and 5A).

567 **Statistical analysis**

568 Results from image-based flow cytometry are presented as boxplots of the pooled
569 fluorescence values for all analyzed cell regions from all donors using the median
570 fluorescence value at each condition divided by the median fluorescence value of
571 the NC condition (*e.g*. Fig S1B). The corresponding calculated Δ% and Δ%A values
572 are presented as mean +/- s.e.m. Differences in these values were assessed using
573 two-way ANOVA, considering capacitation time (*e.g*. NC, 0, 60, 240 min, etc.) as
574 one factor, and treatment (*e.g.* Control, Inh-172, Cl-GBI, etc.) as the second factor.
575 Motility measurements are presented as mean +/- s.e.m. and statistical differences
576 assessed also with two-way ANOVA. The Tukey test was subsequently applied to
577 determine differences between treatments. A probability (*p*) value <0.05 was
578 considered a statistically significant difference. GraphPad Prism version 6
579 (GraphPad, USA) was used for statistical analysis. ggplot2 library (Wickham, 2009)
580 in R studio software (R Core Team, 2017) was employed for plotting and data
581 analysis. The final versions of the figures were prepared using Inkscape 0.91
582 (Inkscape.org, USA).

583 **ACKNOWLEDGMENTS**

584 We thank Paulina Torres, Andres Saralegui, Yoloxóchilt Sánchez and Jose Luis De
585 la Vega for technical assistance. We thank Shirley Ainsworth for library support. We
586 acknowledge Juan Manuel Hurtado, Roberto Rodríguez, Omar Arriaga and Arturo

Ocádiz for computer services. We thank Marcela Trevino for critically reading the manuscript and English editing.

COMPETING INTEREST

The authors declare no competing or financial interests.

FUNDING

This study was supported by DGAPA-UNAM (IN202519 to C.L. Treviño). Matamoros-Volante A., is a student of the Doctorado en Ciencias Bioquímicas-UNAM program supported by CONACyT scholarship.

REFERENCES

Alasmari, W., Costello, S., Correia, J., Oxenham, S. K., Morris, J., Fernandes, L., Ramalho-Santos, J., Kirkman-Brown, J., Michelangeli, F., Publicover, S., et al. (2013). Ca2+ Signals Generated by CatSper and Ca2+ Stores Regulate Different Behaviors in Human Sperm. *J. Biol. Chem.* **288**, 6248–6258.

Alvau, A., Battistone, M. A., Gervasi, M. G., Navarrete, F. A., Xu, X., Sánchez-Cárdenas, C., De la Vega-Beltran, J. L., Da Ros, V. G., Greer, P. A., Darszon, A., et al. (2016). The tyrosine kinase FER is responsible for the capacitation- associated increase in tyrosine phosphorylation in murine sperm. *Development* **143**, 2325–2333.

Austin, C. R. and Sakkas, D. (1951). Observations on the penetration of the sperm in the mammalian egg. *Aust. J. Sci. Res.* **8**, 581–596.

Avenarius, M. R., Hildebrand, M. S., Zhang, Y., Meyer, N. C., Smith, L. L. H., Kahrizi, K., Najmabadi, H. and Smith, R. J. H. (2009). Human Male Infertility Caused by Mutations in the CATSPER1 Channel Protein. *Am. J. Hum. Genet.*

84, 505–510.

Battistone, M. A., Da Ros, V. G., Salicioni, A. M., Navarrete, F. A., Krapf, D., Visconti, P. E. and Cuasnicú, P. S. (2013). Functional human sperm capacitation requires both bicarbonate-dependent PKA activation and down-regulation of Ser/Thr phosphatases by Src family kinases. *Mol. Hum. Reprod.* **19**, 570–80.

Battistone, M. A., Alvau, A., Salicioni, A. M., Visconti, P. E., Da Ros, V. G. and Cuasnicú, P. S. (2014). Evidence for the involvement of proline-rich tyrosine kinase 2 in tyrosine phosphorylation downstream of protein kinase a activation during human sperm capacitation. *Mol. Hum. Reprod.* **20**, 1054–1066.

Bianchini, L., Nanda, A., Wasan, S. and Grinstein, S. (1994). Activation of multiple pH-regulatory pathways in granulocytes by a phosphotyrosine phosphatase antagonist. *Biochem. J.* **301 (Pt 2)**, 539–44.

Brukman, N. G., Nuñez, S. Y., Puga Molina, L. del C., Buffone, M. G., Darszon, A., Cuasnicu, P. S. and Da Ros, V. G. (2019). Tyrosine phosphorylation signaling regulates Ca 2+ entry by affecting intracellular pH during human sperm capacitation. *J. Cell. Physiol.* **234**, 5276–5288.

Buffone, M. G., Ijiri, T. W., Cao, W., Merdiushev, T., Aghajanian, H. K. and Gerton, G. L. (2012). Heads or tails? Structural events and molecular mechanisms that promote mammalian sperm acrosomal exocytosis and motility. *Mol. Reprod. Dev.* **79**, 4–18.

Buffone, M. G., Wertheimer, E. V., Visconti, P. E. and Krapf, D. (2014). Central role of soluble adenylyl cyclase and cAMP in sperm physiology. *Biochim. Biophys. Acta - Mol. Basis Dis.* **1842**, 2610–2620.

635 **Ch'en, F. F.-T., Villafuerte, F. C., Swietach, P., Cobden, P. M. and Vaughan-**
636 **Jones, R. D.** (2008). S0859, an N-cyanosulphonamide inhibitor of sodium-
637 bicarbonate cotransport in the heart. *Br. J. Pharmacol.* **153**, 972–82.
638 **Chang, M.** (1951). Fertilizing Capacity of Spermatozoa deposited into the Fallopian
639 Tubes. *Nature* **168**, 697–698.
640 **Chávez, J. C., Hernández-González, E. O., Wertheimer, E., Visconti, P. E.,**
641 **Darszon, A. and Treviño, C. L.** (2012). Participation of the Cl-/HCO(3)-
642 exchangers SLC26A3 and SLC26A6, the Cl- channel CFTR, and the
643 regulatory factor SLC9A3R1 in mouse sperm capacitation. *Biol. Reprod.* **86**,
644 1–14.
645 **Cross, N. L. and Razy-Faulkner, P.** (1997). Control of human sperm intracellular
646 pH by cholesterol and its relationship to the response of the acrosome to
647 progesterone. *Biol. Reprod.* **56**, 1169–1174.
648 **Damkier, H. H., Nielsen, S. and Praetorius, J.** (2007). Molecular expression of
649 SLC4-derived Na-dependent anion transporters in selected human tissues.
650 *Am J Physiol Regul Integr Comp Physiol* **293**, 2136–2146.
651 **Demarco, I. A., Espinosa, F., Edwards, J., Sosnik, J., de la Vega-Beltrán, J. L.,**
652 **Hockensmith, J. W., Kopf, G. S., Darszon, A. and Visconti, P. E.** (2003).
653 Involvement of a Na + /HCO Cotransporter in Mouse Sperm Capacitation. *J.*
654 *Biol. Chem.* **278**, 7001–7009.
655 **El Khouri, E., Whitfield, M., Stouvenel, L., Kini, A., Riederer, B., Lores, P.,**
656 **Romermann, D., di stefano, G., Drevet, J. R., Saez, F., et al.** (2018).
657 Slc26a3 Deficiency is Associated with Epididymis Dysplasia and Impaired
658 Sperm Fertilization Potential in the Mouse. *Mol. Reprod. Dev.* 1–14.

659 **Foresta, C., Garolla, A., Cosci, I., Menegazzo, M., Ferigo, M., Gandin, V. and**
660 **De Toni, L.** (2014). Role of zinc trafficking in male fertility: From germ to
661 sperm. *Hum. Reprod.* **29**, 1134–1145.
662 **Hereng, T. H., Elgstøen, K. B. P., Eide, L., Rosendal, K. R. and Skålhegg, B. S.**
663 (2014). Serum albumin and HCO3-regulate separate pools of ATP in human
664 spermatozoa. *Hum. Reprod.* **29**, 918–930.
665 **Hernández-González, E. O., Treviño, C. L., Castellano, L. E., de la Vega-**
666 **Beltrán, J. L., Ocampo, A. Y., Wertheimer, E., Visconti, P. E. and Darszon,**
667 **A.** (2007). Involvement of cystic fibrosis transmembrane conductance
668 regulator in mouse sperm capacitation. *J. Biol. Chem.* **282**, 24397–406.
669 **Ho, H.-C., Granish, K. A. and Suarez, S. S.** (2002). Hyperactivated Motility of Bull
670 Sperm Is Triggered at the Axoneme by Ca2+ and Not cAMP. *Dev. Biol.* **250**,
671 208–217.
672 **Hondares, E., Brown, M. A., Musset, B., Morgan, D., Cherny, V. V, Taubert, C.,**
673 **Bhamrah, M. K., Coe, D., Marelli-Berg, F., Gribben, J. G., et al.** (2014).
674 Enhanced activation of an amino-terminally truncated isoform of the voltage-
675 gated proton channel HVCN1 enriched in malignant B cells. *Proc. Natl. Acad.*
676 *Sci. U. S. A.* **111**, 18078–83.
677 **Hong, L., Kim, I. H. and Tombola, F.** (2014). Molecular determinants of Hv1
678 proton channel inhibition by guanidine derivatives. *Proc. Natl. Acad. Sci. U. S.*
679 *A.* **111**, 9971–6.
680 **Hwang, J. Y., Mannowetz, N., Zhang, Y., Everley, R. A., Gygi, S. P.,**
681 **Bewersdorf, J., Lishko, P. V. and Chung, J. J.** (2019). Dual Sensing of
682 Physiologic pH and Calcium by EFCAB9 Regulates Sperm Motility. *Cell* **177**,

1480-1494.e19.

José, O., Torres-Rodríguez, P., Forero-Quintero, L. S., Chávez, J. C., De la Vega-Beltrán, J. L., Carta, F., Supuran, C. T., Deitmer, J. W. and Treviño, C. L. (2015). Carbonic anhydrases and their functional differences in human and mouse sperm physiology. *Biochem. Biophys. Res. Commun.* **468**, 713–718.

Kalina, M., Socher, R., Rotem, R. and Naor, Z. (1995). Ultrastructural localization of protein kinase C in human sperm. *J. Histochem. Cytochem.* **43**, 439–445.

Kirichok, Y., Navarro, B. and Clapham, D. E. (2006). Whole-cell patch-clamp measurements of spermatozoa reveal an alkaline-activated Ca2+ channel. *Nature* **439**, 737–740.

Li, C. Y., Jiang, L. Y., Chen, W. Y., Li, K., Sheng, H. Q., Ni, Y., Lu, J. X., Xu, W. X., Zhang, S. Y. and Shi, Q. X. (2010). CFTR is essential for sperm fertilizing capacity and is correlated with sperm quality in humans. *Hum. Reprod.* **25**, 317–327.

Lishko, P. V. and Kirichok, Y. (2010). The role of Hv1 and CatSper channels in sperm activation. *J. Physiol.* **588**, 4667–4672.

Lishko, P. V., Botchkina, I. L., Fedorenko, A. and Kirichok, Y. (2010). Acid Extrusion from Human Spermatozoa Is Mediated by Flagellar Voltage-Gated Proton Channel. *Cell* **140**, 327–337.

Lishko, P. V, Kirichok, Y., Ren, D., Navarro, B., Chung, J.-J. and Clapham, D. E. (2012). The control of male fertility by spermatozoan ion channels. *Annu. Rev. Physiol.* **74**, 453–75.

Liu, Y., Wang, D.-K. D.-K. and Chen, L.-M. (2012). The Physiology of Bicarbonate

Transporters in Mammalian Reproduction. *Biol. Reprod.* **86**, 99–99.

Lopez-Gonzalez, I., Torres-Rodriguez, P., Sanchez-Carranza, O., Solis-Lopez, A., Santi, C. M., Darszon, A. and Trevino, C. L. (2014). Membrane hyperpolarization during human sperm capacitation. *Mol. Hum. Reprod.* **20**, 619–629.

Mannowetz, N., Wandernoth, P. M. and Wennemuth, G. (2012). Glucose is a pH-dependent motor for sperm beat frequency during early activation. *PLoS One* **7**, e41030.

Marquez, B. and Suarez, S. S. (2007). Bovine Sperm Hyperactivation Is Promoted by Alkaline-Stimulated Ca2+ Influx1. *Biol. Reprod.* **76**, 660–665.

Matamoros-Volante, A., Moreno-Irusta, A., Torres-Rodriguez, P., Giojalas, L., Gervasi, M. G., Visconti, P. E. and Treviño, C. L. (2018). Semi-automatized segmentation method using image-based flow cytometry to study sperm physiology: the case of capacitation-induced tyrosine phosphorylation. *Mol. Hum. Reprod.* **24**, 64–73.

Miller, M. R., Mansell, S. A., Meyers, S. A. and Lishko, P. V (2015). Cell Calcium Flagellar ion channels of sperm : similarities and differences between species. *Cell Calcium* **58**, 105–113.

Miller, M. R., Kenny, S. J., Mannowetz, N., Mansell, S. A., Wojcik, M., Mendoza, S., Zucker, R. S., Xu, K. and Lishko, P. V. (2018). Asymmetrically Positioned Flagellar Control Units Regulate Human Sperm Rotation. *Cell Rep.* **24**, 2606–2613.

Mishra, A. K., Kumar, A., Swain, D. K., Yadav, S. and Nigam, R. (2018). Insights into pH regulatory mechanisms in mediating spermatozoa functions. *Vet.*

World **11**, 852–858.

Morgan, D., Cherny, V. V., Finnegan, A., Bollinger, J., Gelb, M. H. and DeCoursey, T. E. (2007). Sustained activation of proton channels and NADPH oxidase in human eosinophils and murine granulocytes requires PKC but not cPLA $_2$ α activity. *J. Physiol.* **579**, 327–344.

Mortimer, S. T. (2000). CASA—Practical Aspects. *J. Androl.* **21**, 515–524.

Musset, B., Capasso, M., Cherny, V. V., Morgan, D., Bhamrah, M., Dyer, M. J. S. and DeCoursey, T. E. (2010). Identification of Thr29 as a critical phosphorylation site that activates the human proton channel Hvcn1 in leukocytes. *J. Biol. Chem.* **285**, 5117–5121.

Nanda, A. and Grinstein, S. (1995). Chemoattractant-induced activation of vaculoar H+ pumps and of an H+-selective conductance in neutrophils. *J. Cell. Physiol.* **165**, 588–599.

Navarro, B., Kirichok, Y. and Clapham, D. E. (2007). KSper, a pH-sensitive K+ current that controls sperm membrane potential. *Proc Natl Acad Sci U S A* **104**, 7688–7692.

Neuhaus, E. M., Mashukova, A., Barbour, J., Wolters, D., Hatt, H., Giordano, R., Magnano, A. R., Lorenzini, R., Lavia, P. and Spadafora, C. (2006). Novel function of beta-arrestin2 in the nucleus of mature spermatozoa. *J. Cell Sci.* **119**, 3047–56.

Nishigaki, T., José, O., González-Cota, A. L., Romero, F., Treviño, C. L. and Darszon, A. (2014). Intracellular pH in sperm physiology. *Biochem. Biophys. Res. Commun.* **450**, 1149–1158.

Okamura, N., Tajima, Y., Soejima, A., Masuda, H. and Sugita, Y. (1985).

Sodium bicarbonate in seminal plasma stimulates the motility of mammalian spermatozoa through direct activation of adenylate cyclase. *J. Biol. Chem.* **260**, 9699–9705.

Okamura, N., Tajima, Y., Ishikawa, H., Yoshii, S., Koiso, K. and Sugita, Y. (1986). Lowered levels of bicarbonate in seminal plasma cause the poor sperm motility in human infertile patients. *Fertil Steril* **45**, 265–272.

Orta, G., de la Vega-Beltran, J. L., Martín-Hidalgo, D., Santi, C. M., Visconti, P. E. and Darszon, A. (2018). CatSper channels are regulated by protein kinase A. *J. Biol. Chem.* **293**, 16830–16841.

Owen, D. H. and Katz, D. F. (2005). A review of the physical and chemical properties of human semen and the formulation of a semen simulant. *J. Androl.* **26**, 459–469.

Parkkila, S., Rajaniemi, H. and Kellokumpu, S. (1993). Polarized expression of a band 3-related protein in mammalian sperm cells. *Biol. Reprod.* **49**, 326–331.

Puga Molina, L. C., Pinto, N. A., Torres Rodríguez, P., Romarowski, A., Vicens Sanchez, A., Visconti, P. E., Darszon, A., Treviño, C. L. and Buffone, M. G. (2017). Essential Role of CFTR in PKA-Dependent Phosphorylation, Alkalinization, and Hyperpolarization During Human Sperm Capacitation. *J. Cell. Physiol.* **232**, 1404–1414.

Puga Molina, L. C., Pinto, N. A., Torres, N. I., González-Cota, A. L., Luque, G. M., Balestrini, P. A., Romarowski, A., Krapf, D., Santi, C. M., Treviño, C. L., et al. (2018). CFTR/ENaC-dependent regulation of membrane potential during human sperm capacitation is initiated by bicarbonate uptake through NBC. *J. Biol. Chem.* **293**, 9924–9936.

779 **Pushkin, A., Abuladze, N., Newman, D., Lee, I., Xu, G. and Kurtz, I.** (2000). *Two*
780 *C-Terminal Variants of NBC4, a New Member of the Sodium Bicarbonate*
781 *Cotransporter Family: Cloning, Characterization, and Localization*. John Wiley
782 & Sons, Ltd.
783 **Qi, H., Moran, M. M., Navarro, B., Chong, J. A., Krapivinsky, G., Krapivinsky,**
784 **L., Kirichok, Y., Ramsey, I. S., Quill, T. a and Clapham, D. E.** (2007). All
785 four CatSper ion channel proteins are required for male fertility and sperm cell
786 hyperactivated motility. *Proc. Natl. Acad. Sci. U. S. A.* **104**, 1219–23.
787 **R Core Team** (2017). R: A Language and Environment for Statistical Computing.
788 **Ren, D., Navarro, B., Perez, G., Jackson, A. C., Hsu, S., Shi, Q., Tilly, J. L. and**
789 **Clapham, D. E.** (2001). A sperm ion channel required for sperm motility and
790 male fertility. *Nature* **413**, 603–609.
791 **Rotem, R., Pazt, G. F., Homonnait, Z. T., Kalinat, M. and Naor, Z.** (1990).
792 Protein kinase C is present in human sperm: Possible role in flagellar motility.
793 *Proc. Natl. Acad. Sci. USA* **87**, 7305–7308.
794 **Santi, C. M., Martínez-López, P., de la Vega-Beltrán, J. L., Butler, A., Alisio, A.,**
795 **Darszon, A. and Salkoff, L.** (2010). The SLO3 sperm-specific potassium
796 channel plays a vital role in male fertility. *FEBS Lett.* **584**, 1041–6.
797 **Sousa, A. P., Amaral, A., Baptista, M., Tavares, R., Caballero Campo, P.,**
798 **Caballero Peregrín, P., Freitas, A., Paiva, A., Almeida-Santos, T. and**
799 **Ramalho-Santos, J.** (2011). Not all sperm are equal: functional mitochondria
800 characterize a subpopulation of human sperm with better fertilization potential.
801 *PLoS One* **6**, e18112.
802 **Suarez, S. S.** (2008). Control of hyperactivation in sperm. *Hum. Reprod. Update*

14, 647–657.

Touré, A., Lhuillier, P., Gossen, J. A., Kuil, C. W., Lhôte, D., Jégou, B., Escalier, D. and Gacon, G. (2007). The testis anion transporter 1 (Slc26a8) is required for sperm terminal differentiation and male fertility in the mouse. *Hum. Mol. Genet.* **16**, 1783–93.

Ui, M. (1966). A role of phosphofructokinase in pH-dependent regulation of glycolysis. *Biochim. Biophys. Acta - Gen. Subj.* **124**, 310–322.

Wandernoth, P. M., Raubuch, M., Mannowetz, N., Becker, H. M., Deitmer, J. W., Sly, W. S. and Wennemuth, G. (2010). Role of carbonic anhydrase IV in the bicarbonate-mediated activation of murine and human sperm. *PLoS One* **5**, e15061.

Wang, D., King, S. M., Quill, T. A., Doolittle, L. K. and Garbers, D. L. (2003). A new sperm-specific Na+/H+ Exchanger required for sperm motility and fertility. *Nat. Cell Biol.* **5**, 1117–1122.

Wennemuth, G. (2003). Bicarbonate actions on flagellar and Ca2+-channel responses: initial events in sperm activation. *Development* **130**, 1317–1326.

Wennemuth, G., Carlson, A. E., Harper, A. J. and Babcock, D. F. (2003). Bicarbonate actions on flagellar and Ca2+-channel responses: initial events in sperm activation. *Development* **130**, 1317–1326.

Wickham, H. (2009). *ggplot2: Elegant Graphics for Data Analysis*. Springer-Verlag New York.

Xu, W. M., Shi, Q. X., Chen, W. Y., Zhou, C. X., Ni, Y., Rowlands, D. K., Yi Liu, G., Zhu, H., Ma, Z. G., Wang, X. F., et al. (2007). Cystic fibrosis transmembrane conductance regulator is vital to sperm fertilizing capacity and

male fertility. *Proc. Natl. Acad. Sci. U. S. A.* **104**, 9816–21.

Zeng, Y., Oberdorf, J. A. and Florman, H. M. (1996). pH regulation in mouse sperm: identification of Na(+)-, Cl(-)-, and HCO3(-)-dependent and arylaminobenzoate-dependent regulatory mechanisms and characterization of their roles in sperm capacitation. *Dev. Biol.* **173**, 510–520.

Zeng, X.-H., Yang, C., Kim, S. T., Lingle, C. J. and Xia, X.-M. (2011). Deletion of the Slo3 gene abolishes alkalization-activated K+ current in mouse spermatozoa. *Proc. Natl. Acad. Sci. U. S. A.* **108**, 5879–84.

Zeng, X.-H., Navarro, B., Xia, X.-M., Clapham, D. E. and Lingle, C. J. (2013). Simultaneous knockout of Slo3 and CatSper1 abolishes all alkalization- and voltage-activated current in mouse spermatozoa. *J. Gen. Physiol.* **142**, 305–13.

851 **Figure 1**

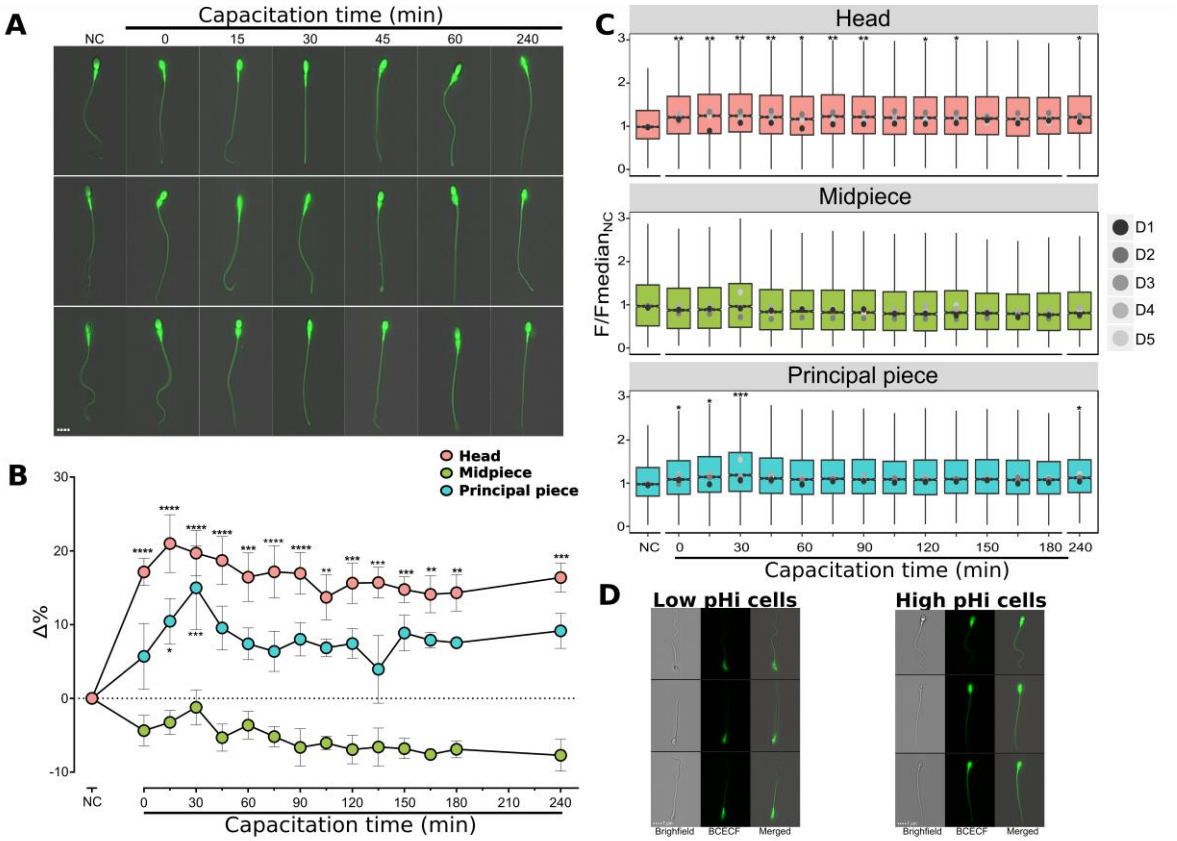

852

853 **Figure 1. Intracellular alkalization during sperm capacitation occurs in the**
854 **head and the principal piece but not in the midpiece**. **A.** Three representative
855 fluorescence images of BCECF-stained human sperm cells either non-capacitated
856 (NC) or at the indicated capacitation times. **B.** Δ% values (Δ%=%T-%NC) for each
857 subcellular region in cells either non-capacitated (NC) or at the indicated capacitation
858 times. Data represent the mean ± s.e.m. (n=5). **C.** Boxplots of normalized BCECF
859 fluorescence values for each subcellular region in cells either non-capacitated (NC)
860 or at the indicated capacitation times. Gray-scale dots (D1-D5) within boxplots
861 indicate the median fluorescence value for the entire sperm population from each
862 donor, consisting of at least 1,000 cells each (n=5). Data were compared by one-
863 way ANOVA considering capacitation time as one factor. Tukey's multiple

comparison test was employed as post hoc analysis. *p<0.05, **p<0.01, ***p<0.001, ****p<0.0001. **D.** Three representative images of cells considered as having high or low pH_i.

888 **Figure 2**

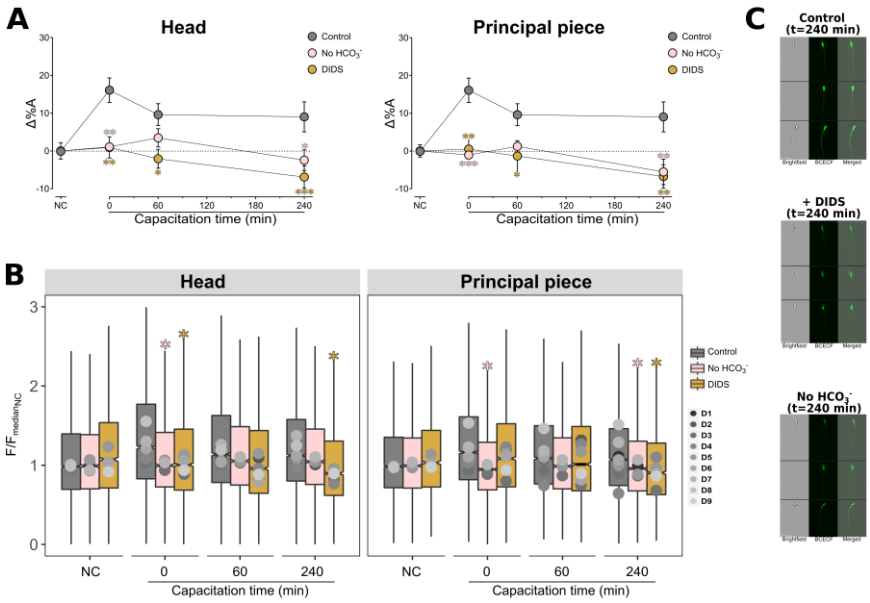

889

890 **Figure 2. HCO_3^- influx is required for the initial and sustained pH_i increase in**
891 **the head and the principal piece**. **A.** Δ%A values (Δ%A=%T-%NC_A) for each
892 subcellular region from human sperm cells placed in non-capacitating medium or in
893 complete capacitating medium and in both media in the presence or absence of 100
894 µM DIDS, or medium lacking HCO_3^- (applies only to capacitating medium). Values
895 were measured at the indicated capacitation times. Data represent the mean ±
896 s.e.m. (n=9 for Control, n=6 for DIDS, n=4 No HCO_3^-). **B.** Boxplots of normalized
897 BCECF fluorescence values for each subcellular region in cells under the same
898 conditions as in **A**. Gray-scale dots (D1-D9) within boxplots indicate the median
899 fluorescence value for the entire sperm population from each donor, consisting of at
900 least 1,000 cells each (n=9 for Control, n=6 for DIDS, n=4 No HCO_3^-). **C**. Three
901 representative images of cells capacitated for 240 min under the indicated
902 conditions. Data were compared using two-way ANOVA with incubation time as one
903 factor, and treatment as the other factor. *p<0.05, **p<0.01, ***p<0.001.

904 **Figure 3**

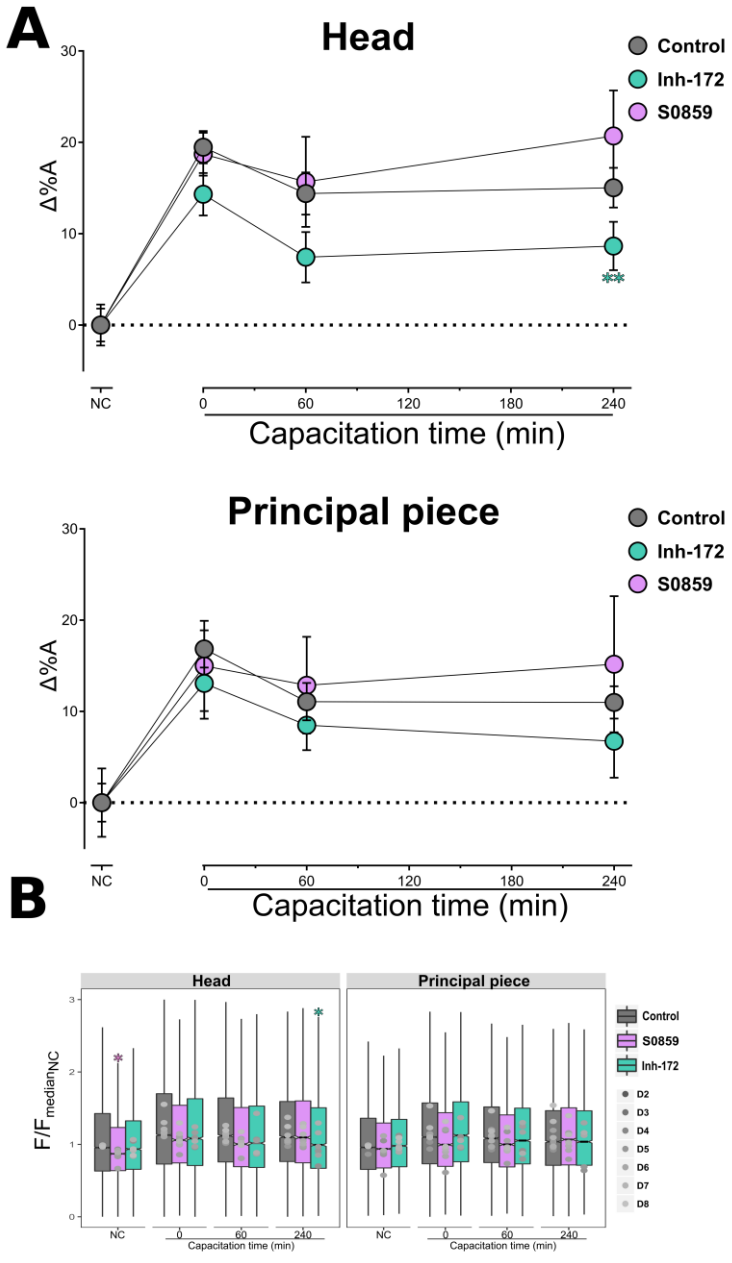

905

906 **Figure 3. NBC and CFTR have a minor role in cytoplasmic alkalization during**

907 **capacitation. A.** Δ%A values (Δ%A=%T-%NC_A) for each subcellular region from

908 human sperm cells placed in non-capacitating medium or in complete capacitating

909 medium and in both media in the presence or absence of 5 μM S0859 or Inh172.

910 Values were measured at the indicated capacitation times. Data represent the mean

± s.e.m. (n=8 for Control and Inh-172, n=6 for S0859). **B.** Boxplots of normalized BCECF fluorescence values for each subcellular region in cells under the same conditions as in **A**. Gray-scale dots (D1-D8) within boxplots indicate the median fluorescence value for the entire sperm population from each donor, consisting of at least 1,000 cells each (n=8 for Control and Inh-172, n=6 for S0859). Data were compared using two-way ANOVA with incubation time as one factor, and treatment as the other factor. *p<0.05, **p<0.01.

935 **Figure 4**

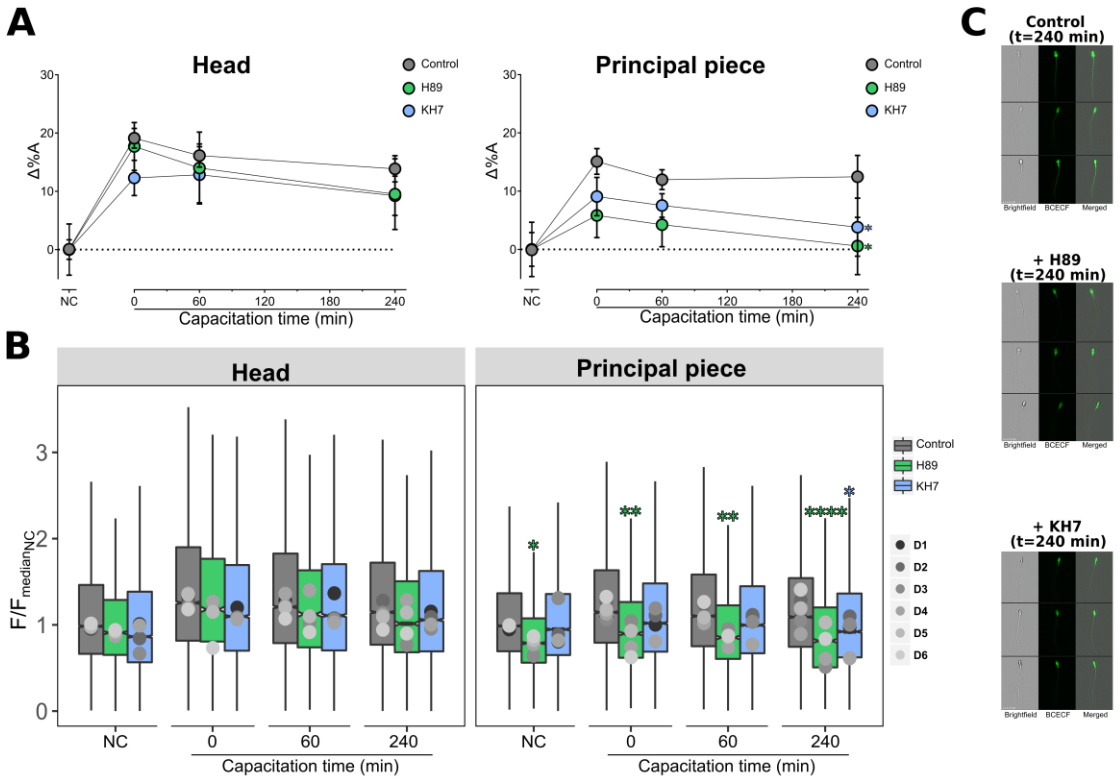

936

937 **Figure 4.** ***The PKA signaling pathway participates in the regulation of***

938 ***capacitation-associated alkalization in the principal piece, but not in the head***.

939 **A.** Δ%A values (Δ%A=%T-%NC_A) for each subcellular region from human sperm

940 cells placed in non-capacitating medium or in complete capacitating medium and in

941 both media in the presence or absence of 50 µM KH7 or 30 µM H89. Values were

942 measured at the indicated capacitation times. Data represent the mean ± s.e.m. (n=6

943 for Control, n=4 for KH7 and H89). **B.** Boxplots of normalized BCECF fluorescence

944 values for each subcellular region in cells under the same conditions as in **A**. Gray-

945 scale dots (D1-D6) within boxplots indicate the median fluorescence value for the

946 entire sperm population from each donor, consisting of at least 1,000 cells each (n=6

947 for Control, n=4 for KH7 and H89). Data were compared using two-way ANOVA with

948 incubation time as one factor, and treatment as the other factor. *p<0.05, **p<0.01,

949 ****p<0.0001.

950

951

952

953

954

955

956

957

958

959

960

961

962

963

964

965

966

967

968

969

970

971

Figure 5

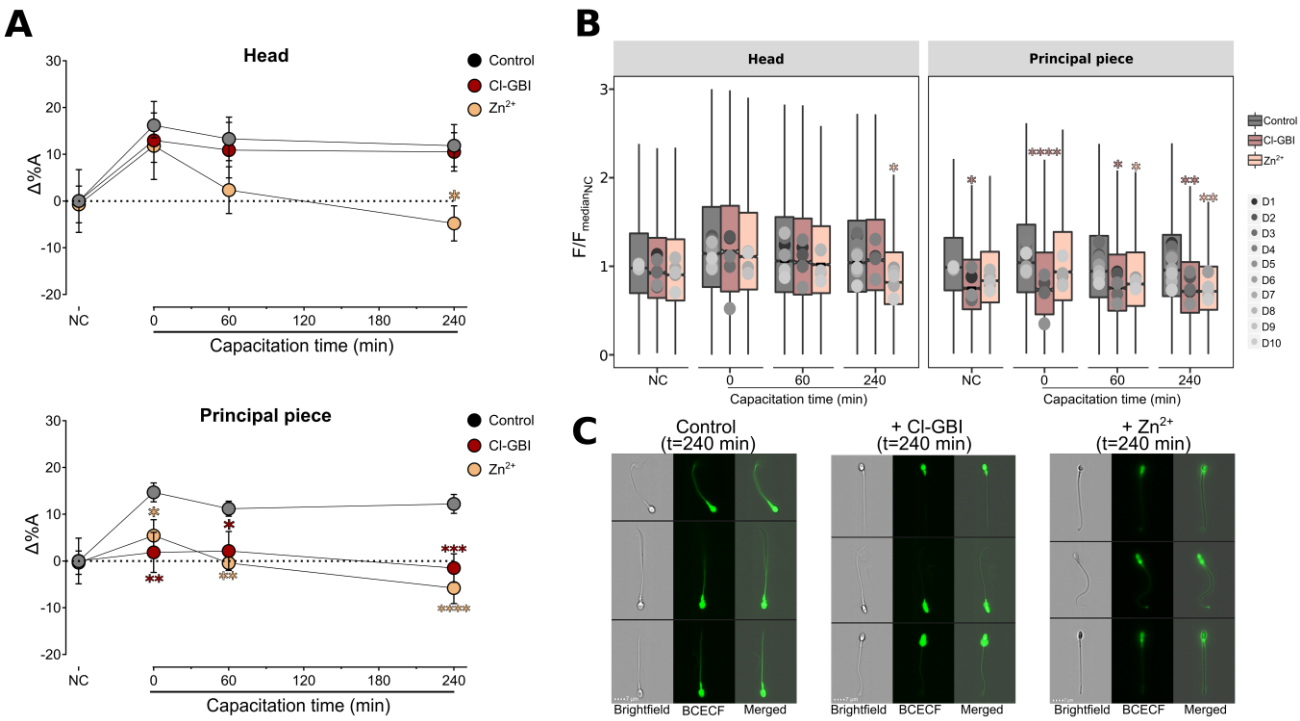

Figure 5*. Inhibition of Hv1 prevented alkalization in the principal piece but not in the head*. A. Δ%A values (Δ%A=%T-%NC_A) for each subcellular region from human sperm cells placed in non-capacitating medium or in complete capacitating medium and in both media in the presence or absence of 200 µM Cl-GBI or Zn^{2+}. Values were measured at the indicated capacitation times. Data represent the mean ± s.e.m. (n=10 control, n=5 for Cl-GBI and Zn^{2+}). **B.** Boxplots of normalized BCECF fluorescence values for each subcellular region in cells under the same conditions as in **A**. Gray-scale dots (D1-D10) within boxplots indicate the median fluorescence value for the entire sperm population from each donor, consisting of at least 1,000 cells each (n=10 control, n=5 for Cl-GBI and Zn^{2+}). **C.** Three representative images of cells capacitated for 240 min under the indicated conditions. Data were compared

using two-way ANOVA with incubation time as one factor, and treatment as the other factor. *p<0.05, **p<0.01, ***p<0.001, ****p<0.0001.

Figure 6

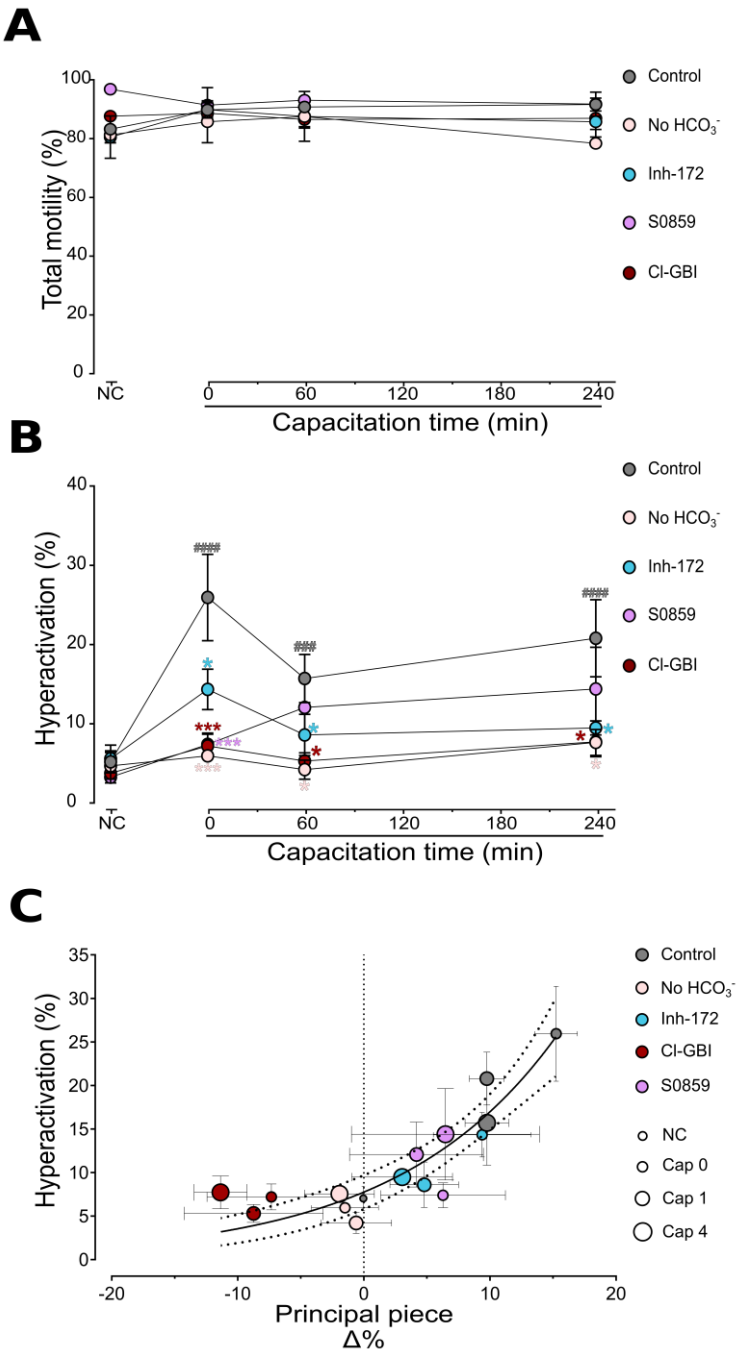

Figure 6. Proteins involved in pH_i control are required for hyperactivated motility but not for total motility. **A.** Total motility measurements of human sperm cells placed in non-capacitating medium or in complete capacitating medium and in

both media in the presence or absence of 5 µM S0859 or Inh172, or 200 µM Cl-GBI at different times of incubation. Data represent the mean ± s.e.m. (n = 5 for Control and Inh-172, n = 4 for Cl-GBI, S0859 and No HCO_3^-). **B.** Quantification of proportion of hyperactive cells during the time and conditions mentioned in A. Data represent the mean ± s.e.m. (n = 5 for Control and Inh-172, n = 4 for Cl-GBI, S0859 and No HCO3 Data were compared using two-way ANOVA with incubation time as one factor, and treatments as the other factor. *p<0.05, ***p<0.001. $^{###}p$<0.001, $^{####}p$<0.0001. C. Changes in hyperactivation as a function Δ%. The incubation time (NC, capacitation at 0, 60 and 240 min) are depicted as increasing size circles. Solid line indicates the exponential fit (fit parameters are indicated in main text). Dotted line are the 95% confidence intervals. Data represent the mean ± s.e.m.